Weakening Solvation via Dipole Interactions Enables Efficient and Stable Perovskite Solar Cells

Shui Li,[1] Han Qin,[1] Mengnan Zuo,[1] Wangbo Xu, Yingdong Xia,[1] Lingfeng Chao,[1*] Yonghua Chen[1*]

[1]State Key Laboratory of Flexible Electronics (LoFE) & Institute of Advanced Materials (IAM), School of Flexible Electronics (Future Technologies), Nanjing Tech University (NanjingTech), 30 South Puzhu Road, Nanjing 211816, Jiangsu, China.

*Corresponding author. Email: iamlfchao@njtech.edu.cn (L.C.); iamyhchen@njtech.edu.cn (Y.C.);

Experimental Section

Materials

Fluorine-doped tin oxide (FTO), lead iodide (PbI_2), methylammonium chloride (MACl), bis (trifluoromethane) sulfonimide lithium salt (Li-TFSI, 99.95%), 4-tertbutyl-pyridine (tBP, 99.9%) and Spiro-OMeTAD were purchased from Advanced Election Technology Co., Ltd. Tin oxide (SnO_2) colloid precursor (15% in H_2O colloidal dispersion) was purchased from Alfa Aesar. Formamidinium iodide (FAI, 99.9%) was purchased from Great Cell Solar. Diethyl ether (Et_2O, 99%) was purchased from Yonghua Chemical Co., Ltd. Dimethylformamide (DMF, 99.7%), dimethyl sulfoxide (DMSO), chlorobenzene (CB, 99.7%), isopropanol (IPA, 99.7%), acetonitrile (ACN, 99.9%) and ethanol were purchased from Sigma Aldrich. Unless otherwise noted, all materials were used as received without further modifications.

Device fabrication

Fluorine-doped tin oxide (FTO) coated glass substrates (purchased from Youxuan Technology Co., Ltd.) were sequentially cleaned with ethanol via ultrasonication,then dried with a nitrogen gun and treated with UV ozone for 20 minutes, respectively. The SnO_2 aqueous solution (diluted 6 times with deionized water) was spin-coated on the cleaned substrates at 4000 rpm for 30 seconds and then annealed at 150 °C for 30 minutes in ambient air. A 1.7M $FAPbI_3$ perovskite precursor solution with 10% excess PbI_2 was prepared by mixing stoichiometric FAI and PbI_2, and MACl in a mixed solvent of DMF and DMF/PAAC (9:1, v/v), which was thoroughly stirred at 20 °C for 6 hours. For perovskite film deposition, 5 μL of precursor solution was blade-coated on FTO/SnO_2 substrates at 70 mm/s, followed by immediate solvent extraction under a vacuum of 0.1 MPa for 90 s. Thermal annealing was performed using a two-step protocol: initial drying at 70°C for 1 min followed by crystallization at 150°C for 15 min. The hole transport layer (HTL) was deposited by spin-coating at 3,000 rpm. for 30 s using a 0.1 M The

Spiro-OMeTAD (dissolved in CB solution, 72.6 mg/mL) with 28.8 μL of 4-tert-butylpyridine and 17.6 μL of Li-TFSI (dissolved in acetonitrile, 520 mg/mL) was spin-coated at the OAI layer at 2500 rpm for 30 s. Finally, the devices were transferred to a vacuum chamber for the thermal evaporation of MoO_3 (5 nm) and Ag (100 nm) under a vacuum of 5×10^{-4} Pa.

Characterizations

The ATR-FTIR spectra were measured by a Thermo Fisher IS50 equipped with a reflectance accessory. Proton nuclear magnetic resonance (NMR) spectra were measured with a JOEL NMR spectrometer (JNM-ECZ400S, 400 MHz Japan). Carbon nuclear magnetic resonance (NMR) spectra were measured with a JOEL NMR spectrometer (JNM-ECZ400S, 400 MHz Japan). Dynamic light scattering (DLS) experiments were performed using a Malvern Zetasizer Nano instrument. Zetapotential measurements were performed using a Malvern Zetasizer Nano instrument. Thermal Gravimetric (TG) measurements were performed using a Mettler Toledo TGA 2(SF). Scanning electron microscopy (SEM) analysis was performed on a SU8010 electron microscope. SEM images were captured using a 5-kV acceleration voltage and an aperture size of 20 μm. Grazing-incidence wide-angle X-ray scattering (GIWAXS) was performed at the BL14BL beamline of the Shanghai Synchrotron Radiation Facility (SSRF) using X-ray with a wavelength of 1.24 Å. Steady-state photoluminescence (PL) spectra and Time-resolved photoluminescence (TRPL) spectra were obtained by FLS1000. The excitation wavelength was set as 520 nm. The TRPL decay data were modeled by a biexponential formula: $Y+A1\exp(-t/\tau1) +A2\exp(-t/\tau2)$. X-ray diffraction (XRD) patterns were performed using Cu Kα radiation as the X-ray source by a Smart Lab diffractometer from Japan. Photo current-voltage (J-V) curves were measured by using 2400 Series Source Meter (Keithley Instruments) under a SS-F5-3A solar simulator (AM 1.5G, 100 mW cm^{-2}) (Enlitech) calibrated by a NREL standard Si cell, and no additional UV filter equipment was used.

Space charge limited current (SCLC) analysis

The structure of a single charge-carrier device is FTO/SnO_2/$FAPbI_3$/$PC_{61}BM$/ C_{60}/ BCP/Ag. The trap density of the perovskite film is calculated with the formula of equation (1)

$$n_{trap} = 2\varepsilon_0 \varepsilon V_{TFL}/(qL^2) \quad (1)$$

where ε_0 is the vacuum permittivity, ε is the relative dielectric constant of perovskite film (46.9 for $FAPbI_3$), q is the elemental charge and L is the thickness of the perovskite layer.

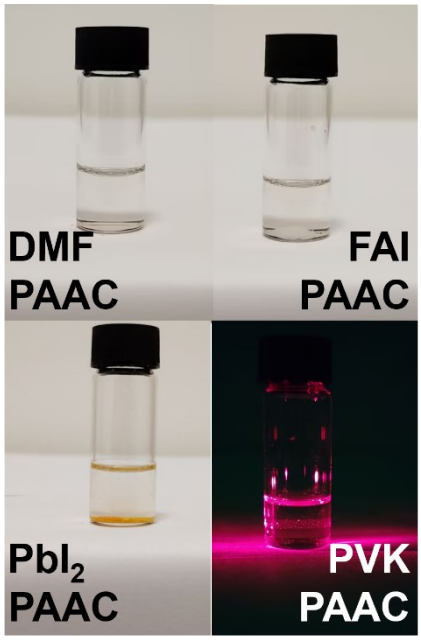

Supplementary Fig. 1 Photograph of the FAI, PbI_2, DMF and perovskite precursor solution with Pentyl propionate.

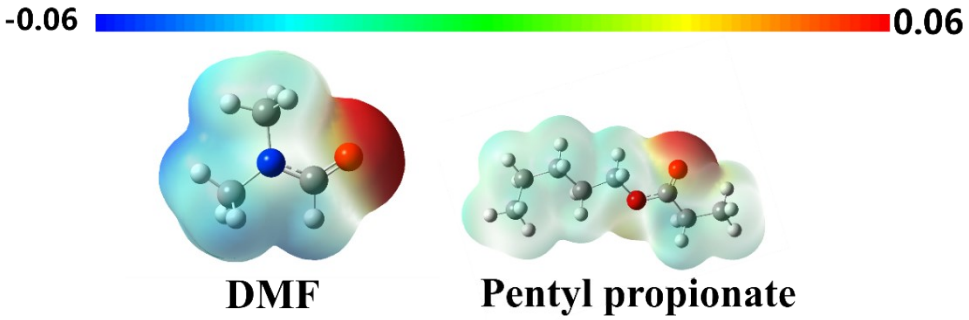

Supplementary Fig. 2 The ESP mapping of DMF and Pentyl propionate.

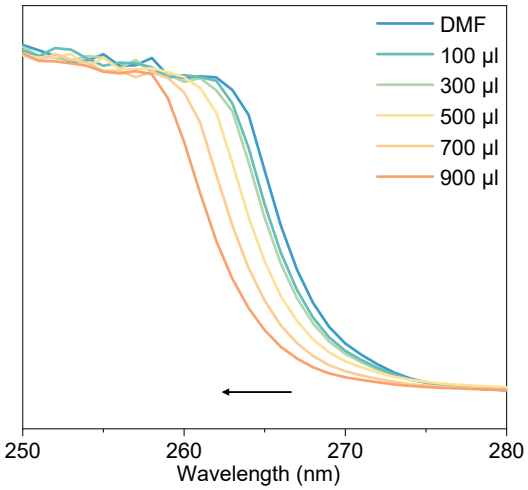

Supplementary Fig. 3 UV-vis spectra of DMF with different contents of Pentyl propionate.

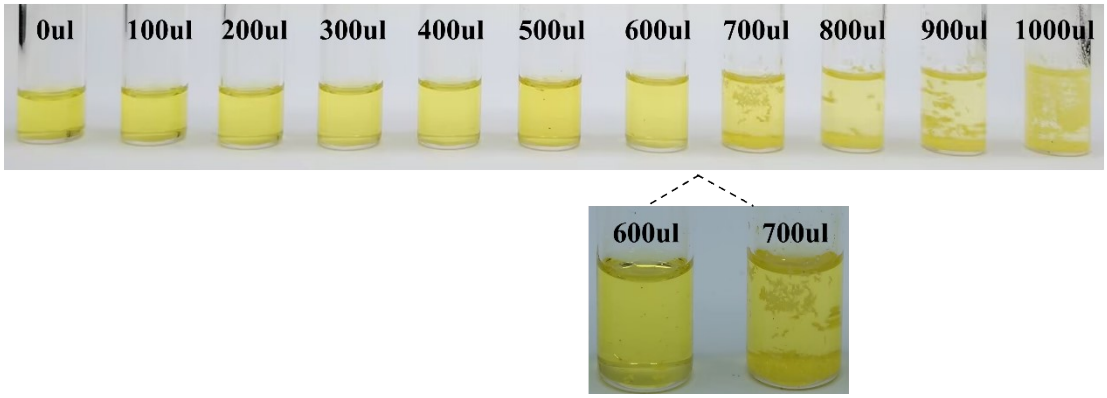

Supplementary Fig. 4 Photograph of adding 1ml pentyl propionate into 1 ml DMF solution of PbI_2 in 100µl increments starting from 0µl.

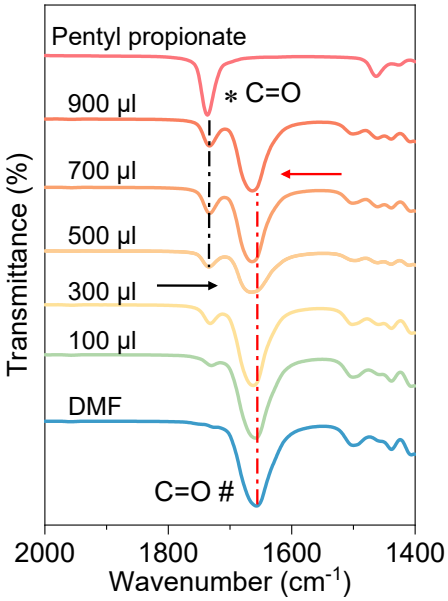

Supplementary Fig.5 FTIR spectra of the C=O of the solution of DMF with different contents of Pentyl propionate.

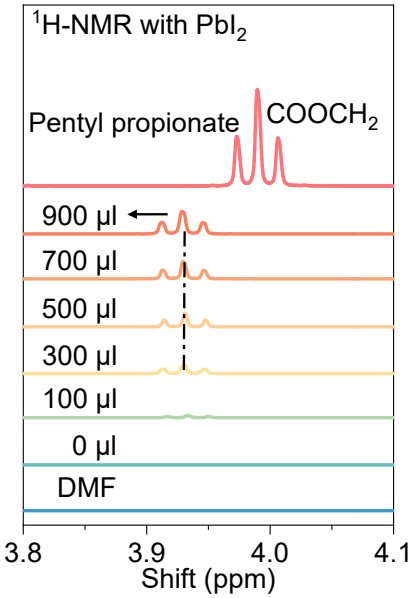

Supplementary Fig.6 ^{1}H-NMR spectra of $COOCH_2$ the solution of PbI_2 dissolved in DMF with different contents of Pentyl propionate.

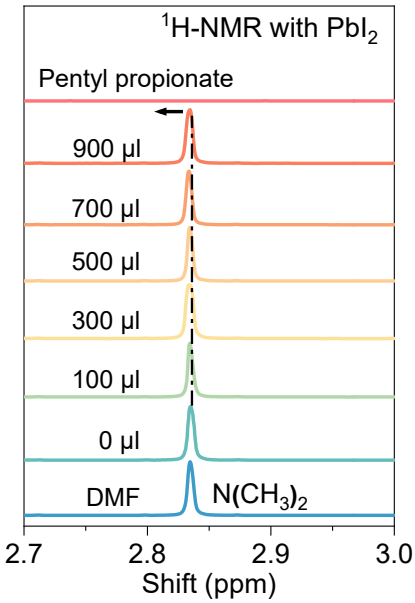

Supplementary Fig. 7 ^{1}H-NMR spectra of the protons of $N(CH_3)_2$ of PbI_2 dissolved in DMF with different contents of Pentyl propionate.

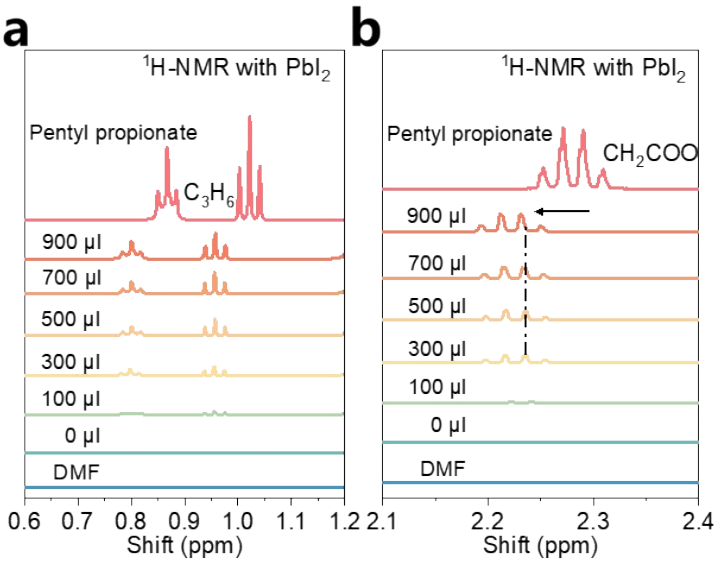

Supplementary Fig. 8 (a) ^{1}H-NMR spectra of the protons of C_3H_6 of PbI_2 dissolved in DMF with different contents of Pentyl propionate. **(b)** ^{1}H-NMR spectra of the protons of CH_2COO of PbI_2 dissolved in DMF with different contents of Pentyl propionate.

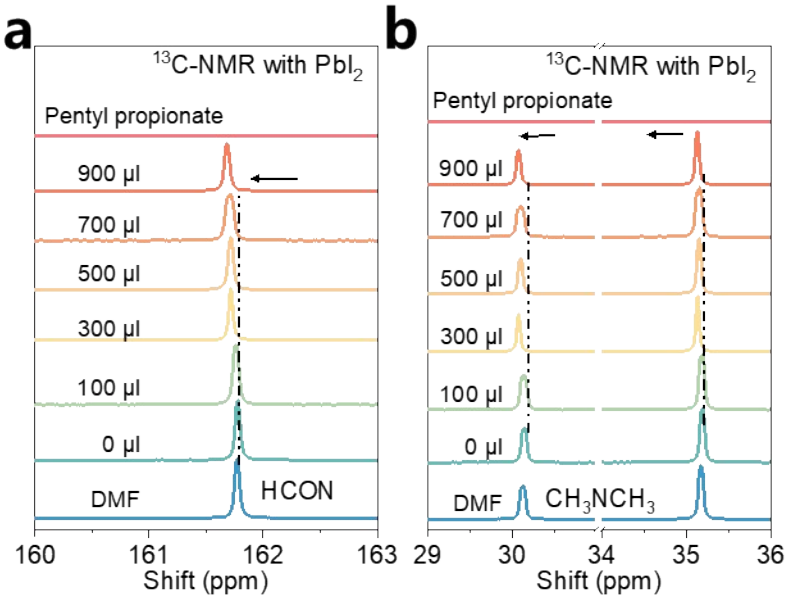

Supplementary Fig. 9 (a) ^{13}C-NMR spectra of the C proton of the amide group HCON of PbI_2 dissolved in DMF with different contents of Pentyl propionate. **(b)** ^{13}C-NMR spectra of the C proton of the amide group $N(CH_3)_2$ of PbI_2 dissolved in DMF with different contents of Pentyl propionate.

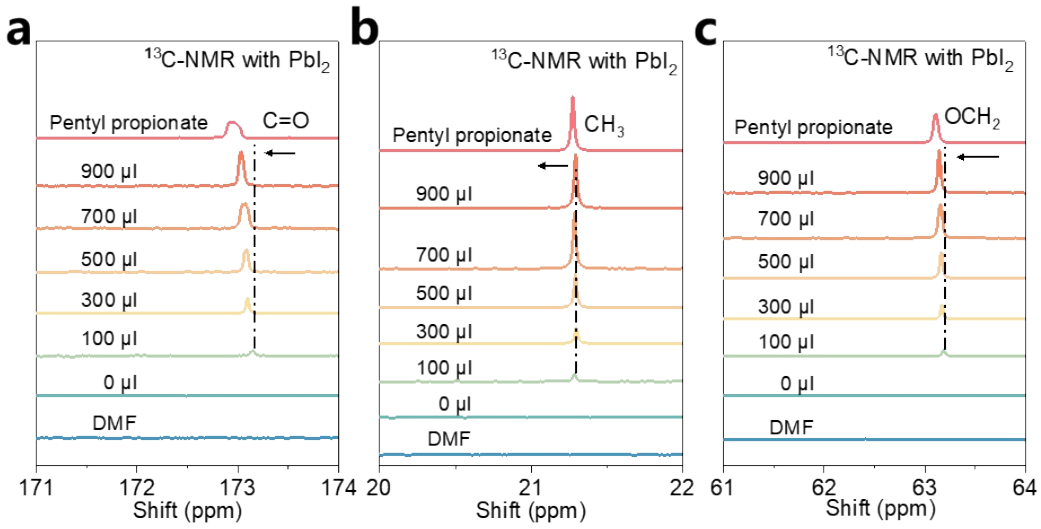

Supplementary Fig. 10 (a) ^{13}C-NMR spectra of the C proton of the amide group COOH of PbI_2 dissolved in DMF with different contents of Pentyl propionate. **(b)** ^{13}C-NMR spectra of the C proton of theCH_3 of PbI_2 dissolved in DMF with different contents of Pentyl propionate. **(b)** ^{13}C-NMR spectra of the C proton of the OCH_2 of PbI_2 dissolved in DMF with different contents of Pentyl propionate.

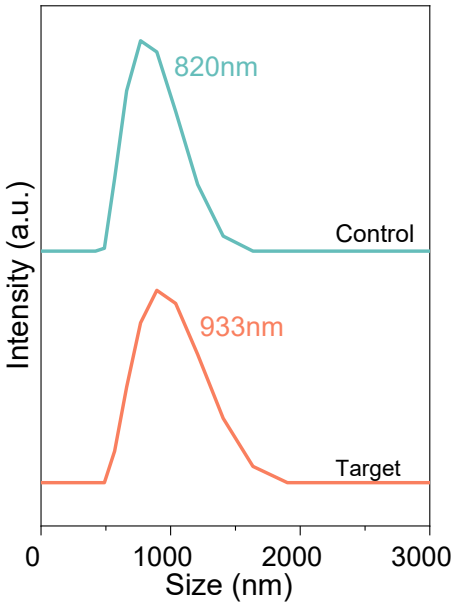

Supplementary Fig. 11 Dynamic Light Scattering (DLS) of the DMF perovskite precursor solution and the PAAC /DMF perovskite precursor solution.

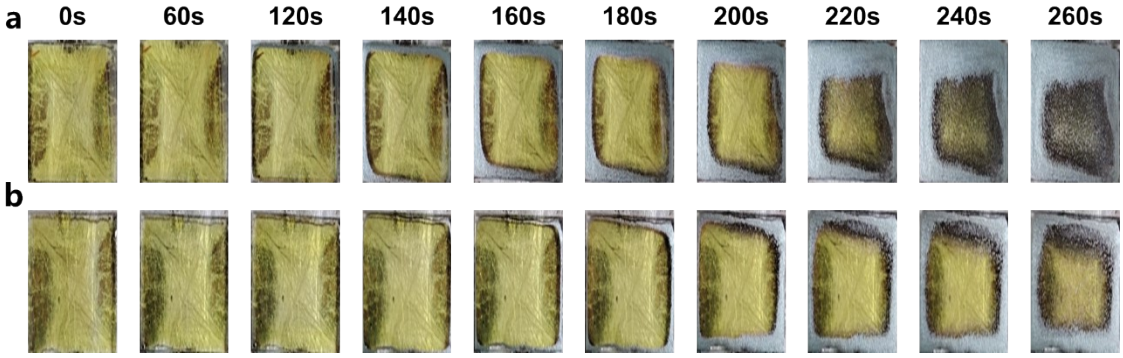

Supplementary Fig. 12 Photograph of the phase transformation of time under constant temperature for (a) the control and (b) the target film.

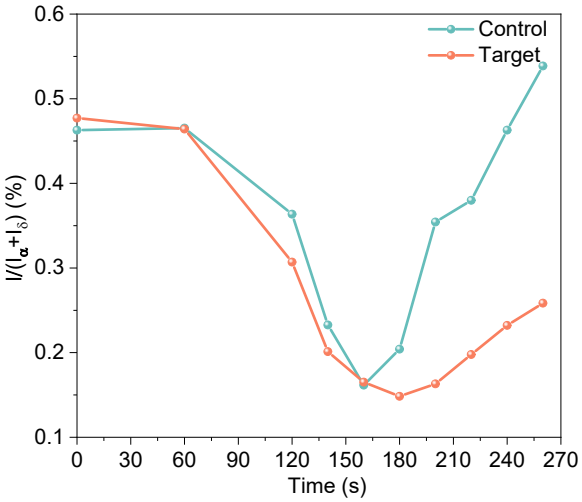

Supplementary Fig. 13 The relative intensity of the α-$FAPbI_3$ XRD diffraction peak.

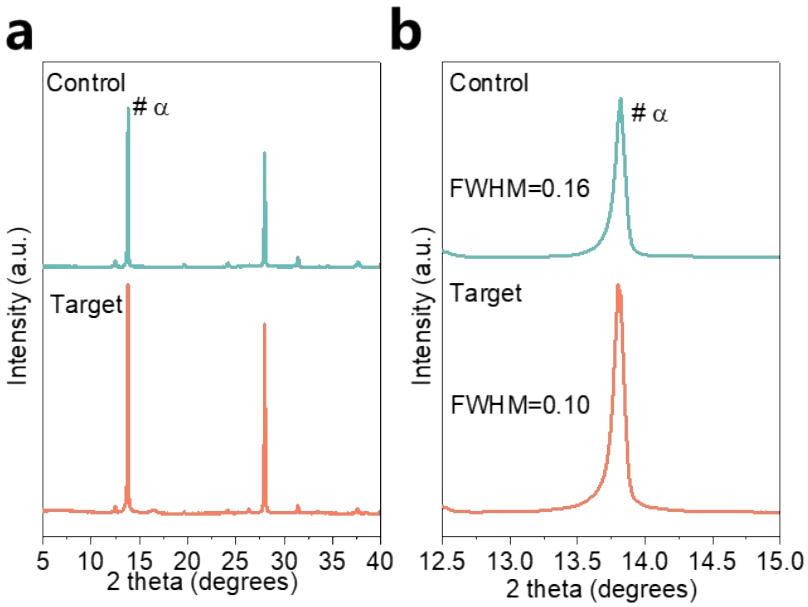

Supplementary Fig. 14 (a) The XRD patterns of control film and target film. **(b)** The half-peak width (FWHM) of the XRD patterns of α-$FAPbI_3$ of control film and target film.

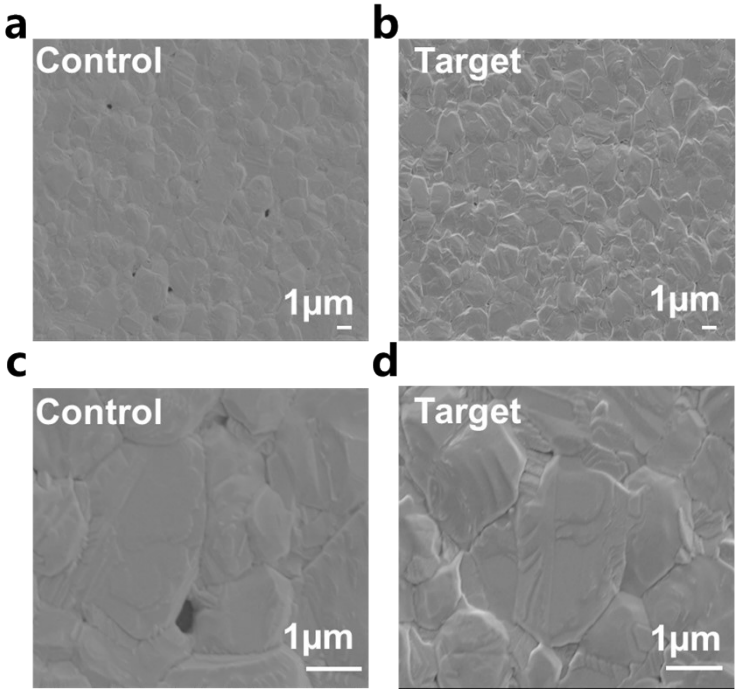

Supplementary Fig. 15 SEM images of **(a)** the control film and **(b)** the target film in 5000 SEM images of **(c)**the control film and **(d)** the target film in 20000.

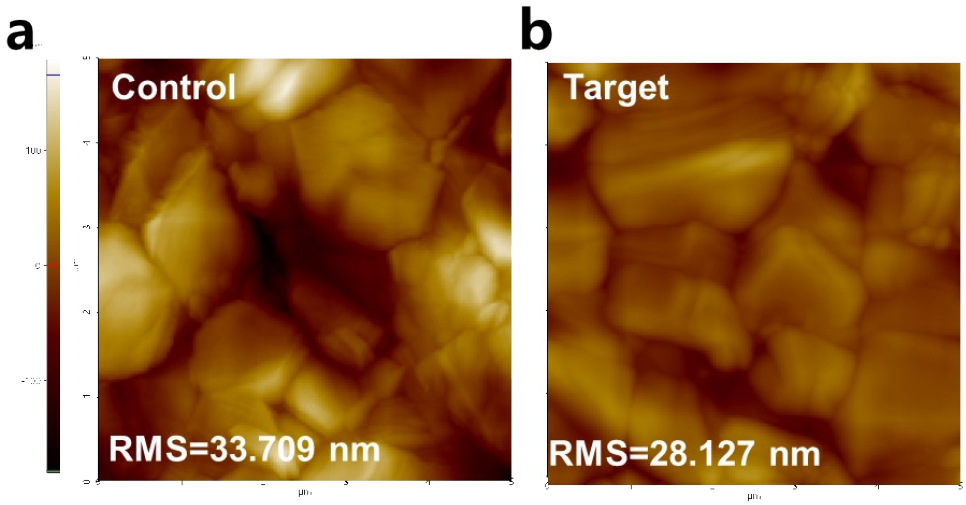

Supplementary Fig. 16 (a) AFM images of the control film **(b)** AFM images of the target film.

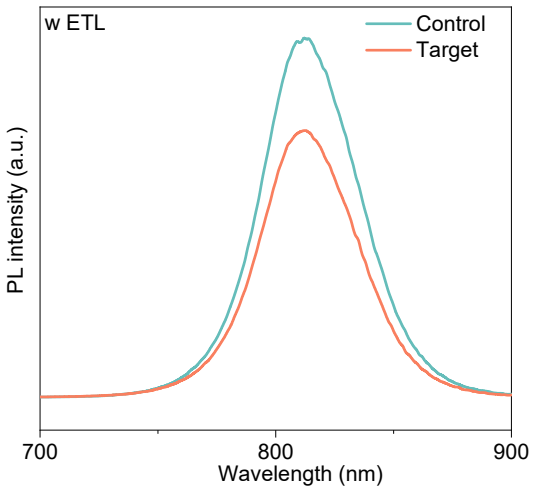

Supplementary Fig. 17 PL of the control film and the target film with ETL.

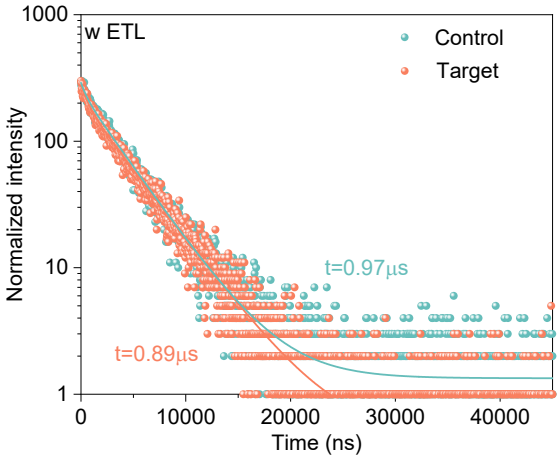

Supplementary Fig. 18 TRPL of the control film and the target film with ETL.

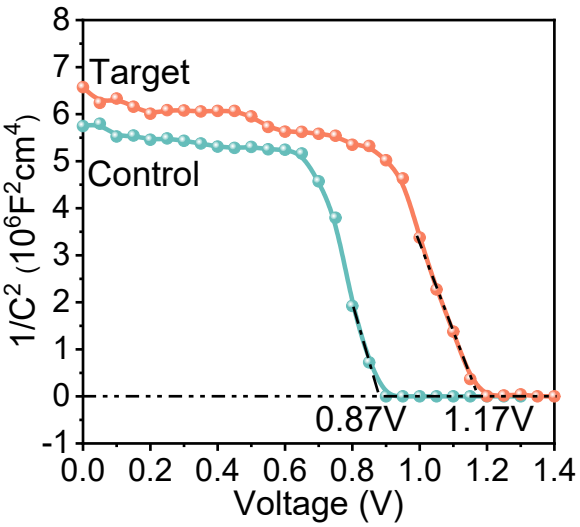

Supplementary Fig. 19 Mott-Schottky curve of control and target PSCs.

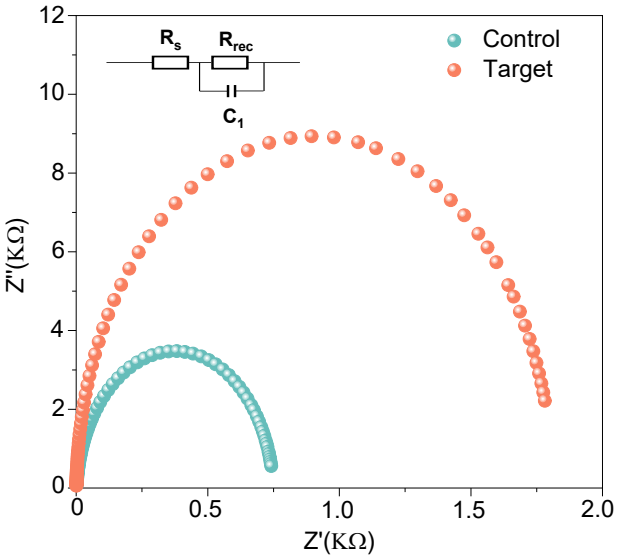

Supplementary Fig. 20 EIS of the control device and the target device.

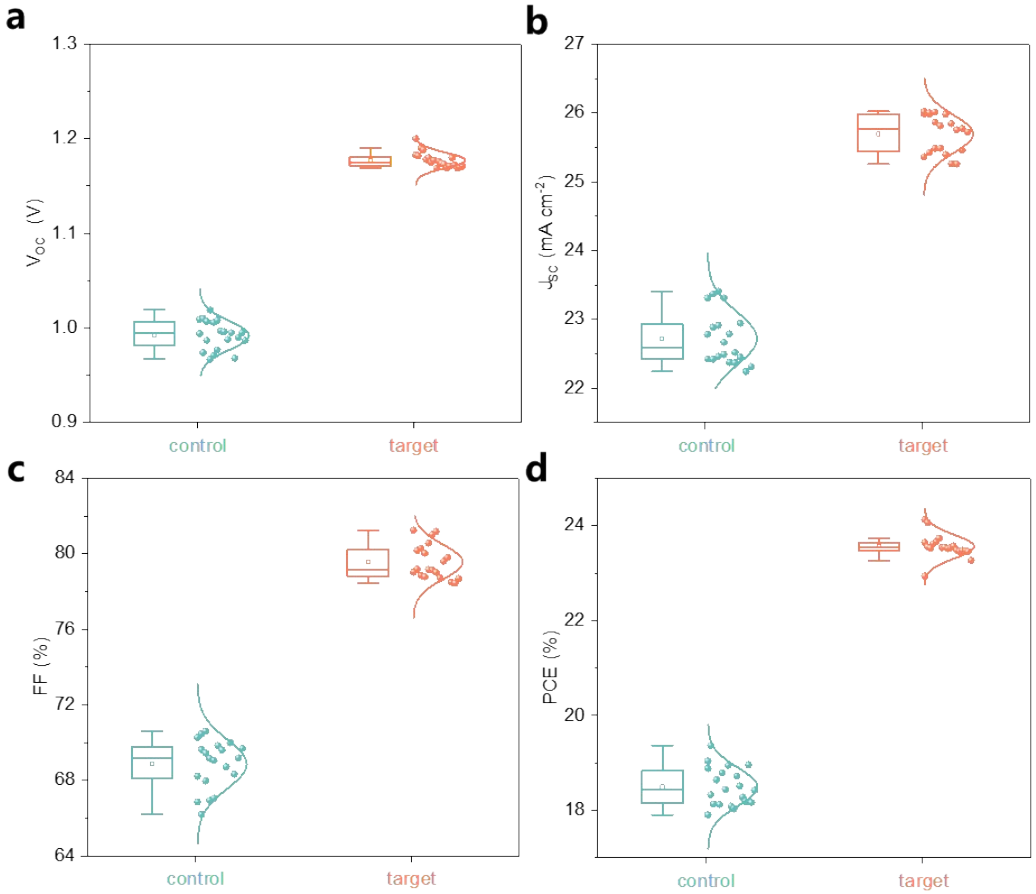

Supplementary Fig. 21 (a) V_{oc}, **(b)** J_{sc}, **(c)** FF and **(d)** PCE distributions of control and target PSCs. The number of devices for each type is 20. The average Voc of control PSCs is 0.99 V and target PSCs is 1.17 V.

Table S1. Detailed parameters of large-area module (5 × 5 cm^2) (area = 12.6 cm^2, number of sub-cells=6)

Sample	V_{oc} (V)	J_{sc} (mA/cm^2)	FF (%)	PCE (%)
Control	5.93	3.93	56.5	13.17
Target	6.75	3.84	77.16	20.06